



HAL
open science

The ExoMars 2028 WISDOM antenna assembly: Description and characterization

Wolf-Stefan Benedix, Sebastian Hegler, Christoph Statz, Ronny Hahnel, Dirk Plettemeier, Valérie Ciarletti

► To cite this version:

Wolf-Stefan Benedix, Sebastian Hegler, Christoph Statz, Ronny Hahnel, Dirk Plettemeier, et al.. The ExoMars 2028 WISDOM antenna assembly: Description and characterization. *Planetary and Space Science*, 2024, 253 (November), pp.105995. 10.1016/j.pss.2024.105995 . insu-04774016v2

HAL Id: insu-04774016

<https://insu.hal.science/insu-04774016v2>

Submitted on 15 Dec 2024

HAL is a multi-disciplinary open access archive for the deposit and dissemination of scientific research documents, whether they are published or not. The documents may come from teaching and research institutions in France or abroad, or from public or private research centers.

L'archive ouverte pluridisciplinaire **HAL**, est destinée au dépôt et à la diffusion de documents scientifiques de niveau recherche, publiés ou non, émanant des établissements d'enseignement et de recherche français ou étrangers, des laboratoires publics ou privés.



Contents lists available at ScienceDirect

Planetary and Space Science

journal homepage: www.elsevier.com/locate/pss

The ExoMars 2028 WISDOM antenna assembly: Description and characterization

Wolf-Stefan Benedix^{a,*}, Sebastian Hegler^a, Christoph Statz^a, Ronny Hahnel^a, Dirk Plettemeier^a, Valérie Ciarletti^b

^a Chair for RF and Photonics Engineering, Communications Lab, Faculty of Electrical Engineering and Computer Engineering, Technische Universität Dresden, 01062 Dresden, Germany

^b LATMOS Université Versailles St-Quentin, CNRS/INSU; LATMOS-IPSL, France

ARTICLE INFO

Keywords:

WISDOM
Antenna
ExoMars 2028
Rosalind Franklin rover
Ground-penetrating radar (GPR)

ABSTRACT

While ground penetrating radars have been extensively researched on Earth, the high-resolution exploration and imaging of the shallow subsurface of celestial bodies in our solar system is still in its early stages, with only a handful of systems capable of the task.

Designing high-resolution radar systems can be a complex task due to the large frequency bandwidth required by the antennas to achieve high vertical resolution. The WISDOM GPR, as part of the 2028 ExoMars mission, is a highly capable and challenging instrument in this context, given its fully-polarimetric setup and mission constraints on the operating environment, robustness, as well as mass and size budget.

This paper outlines the development and characterization process of the WISDOM antenna assembly, which can serve as a model for future radar systems. Furthermore, it presents the results of the antenna characterization as the foundation for instrument calibration and optimal radar sounding outcomes.

1. Introduction

Ground penetrating radar is a well established tool to non-invasively explore the structure and geology of the earth's subsurface (Daniels, 2004). Besides geology, this technique has spread over a variety of fields such as archaeology, mine detection and structural engineering. Depending on the different needs, in terms of penetration depth, resolution, and structures to be detected, a multiplicity of sounding radars were developed to operate over a specific frequency band, which, in turn, drives the design of the antenna system that ensures the necessary transmission and reception of the electromagnetic waves. But these applications are mostly operated on earth, which facilitates a wide range of antenna concepts with respect to mechanical and electrical requirements. For the investigation of the subsurface of other celestial bodies, however, the number of instruments used so far is rather limited.

By now, there are three ground based radars on moon (Fang et al., 2014; Li et al., 2020; Xiao et al., 2019) and two on Mars (Hamran et al., 2020; Zhou et al., 2020). All other radars were placed in orbit, and particularly the subsurface of Mars is mainly sounded by the missions MARSIS and SHARAD. The instrument "Mars Advanced Radar for Subsurface and Ionosphere Sounding" (MARSIS) on MarsExpress works

in four bands each of 1 MHz bandwidth covering a total frequency range from 1.3 MHz to 5.5 MHz and provides a depth resolution of 50 m to 100 m within the subsurface depending on the electrical properties of the sounded materials. These data are supplemented by the measurements of the Shallow Radar (SHARAD) on Mars Reconnaissance Orbiter, which operates over a bandwidth from 15 MHz to 25 MHz and achieves a depth resolution of 10 m to 20 m (Flamini et al., 2007).

These radars allowed a relatively deep sounding of Mars' subsurface but to the cost of a comparatively low resolution. Basically, there is a trade-off between penetration depth, which is higher for low frequencies, and the vertical resolution, which is higher at high frequencies (Daniels, 2004).

Recently, different features of the shallow-subsurface have become the focus of research, because they are suspected to harbour traces of past or present life (Ciarletti et al., 2017). However, the size of these features are far below the resolution of the low frequency sounding orbital radars and hence, the usage of high frequency, broadband radar systems is needed.

For that, some efforts have been made lately to operate ground penetrating radars on other celestial bodies (Moon and Mars so far) with high frequencies, e. g.:

* Corresponding author.

E-mail addresses: wolf-stefan.benedix@tu-dresden.de (W.-S. Benedix), dirk.plettemeier@tu-dresden.de (D. Plettemeier), valerie.ciarletti@latmos.ipsl.fr (V. Ciarletti).

<https://doi.org/10.1016/j.pss.2024.105995>

Received 4 July 2024; Received in revised form 1 October 2024; Accepted 28 October 2024

Available online 6 November 2024

0032-0633/© 2024 The Authors. Published by Elsevier Ltd. This is an open access article under the CC BY-NC-ND license (<http://creativecommons.org/licenses/by-nc-nd/4.0/>).

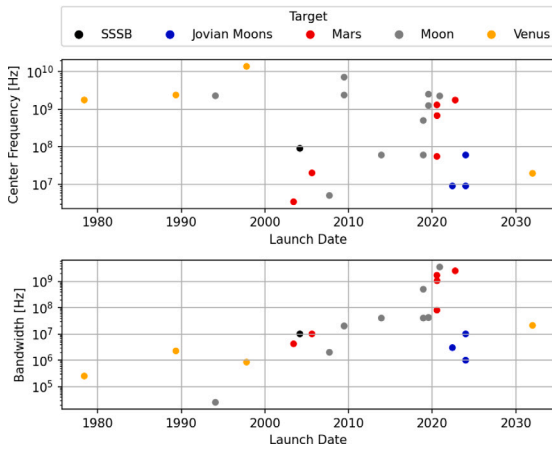


Fig. 1. Bandwidth and centre frequency of radars for specific solar system targets (Ciarletti, 2016).

- WISDOM aboard the rover “Rosalind Franklin” of the mission ExoMars employs a Stepped Frequency Modulated Continuous Wave (SFMCW) radar within the range from 0.5 GHz to 3 GHz with two linear polarizations. The initial design of the antenna system was presented in Ciarletti et al. (2011) and Ciarletti et al. (2011).
- RIMFAX on the rover Perseverance that landed in February 2021 in Jezero Crater applies a gated FMCW radar in the range from 150 MHz to 1200 MHz with a linear polarized antenna (Hamran et al., 2015).
- RoSPR on the rover of Tianwen-1 uses two frequency ranges (from 15 MHz to 95 MHz and from 0.45 GHz to 2.15 GHz) both with gated FMCW and its antenna system bases on that of WISDOM (Zhou et al., 2020). For the high band a dual polarized antenna system is constructed as well but with mechanically separated antennas.

A graphical classification of centre frequency and bandwidth of some past, present and future missions are given in Fig. 1 based on Ciarletti (2016). As one can see: with the present and future missions to Mars and the Moon, the frequency bandwidth rises to achieve a high-resolution image of the subsurface.

Although the higher resolution enables a more detailed characterization of sub-surface structures, important information regarding the roughness and scattering properties cannot directly be obtained from conventional radars. In order to close this knowledge gap, polarimetric radar systems can be employed and are widely used in earth based observation to obtain information on the shape of the reflectors detected in the subsurface or on roughness at the buried interfaces.

In this paper we focus on the design of a fully polarimetric antenna that is capable to probe the shallow subsurface in the frequency range from 0.5 GHz to 3 GHz as well as to withstand the harsh conditions during the journey to and the operations on a place beyond earth. The here proposed antenna is part of the Water Ice Subsurface Deposit Observation on Mars (WISDOM) Ground Penetrating Radar (GPR) aboard the rover “Rosalind Franklin” (European Space Agency, 2019a) on the mission ExoMars (European Space Agency, 2019b).

WISDOM (Ciarletti et al., 2017) is a purpose-built GPR for sounding the subsurface of Mars, recording geological features down to a depth of 3 m to 10 m, depending on the material characteristics (i. e., permittivity, conductivity, and associated losses) of the subsurface. WISDOM will perform radar soundings in order to map the general stratigraphy of the subsurface along the rover path, to detect outcrops, sedimentary deposits, and buried objects (e. g., boulders) to understand the geological history. The results of this sounding will also be used for operational safety assessments for the ExoMars drill, capable of

Table 1
WISDOM Antennas Assembly requirements.

Electrical parameters	
Frequency range	0.5 GHz to 3.0 GHz
Input RF power	20 dBm
Reflection on a 50 Ω line	≤ -10 dB
($ S_{11} $)	
Direct coupling	< -15 dB
Polarization	Two linear, perpendicular polarizations for transmitting and receiving antenna each
Antenna pattern	
HPBW	$\theta > 20^\circ$, $\theta_{H\text{-plane}} > \theta_{E\text{-plane}}$
Gain in main beam direction	> 0 dBi, increasing with frequency
Structural & environmental parameters	
Mass	400 g
Envelope	410 \times 200 \times 200 mm
First mechanical eigenfrequency	> 140 Hz
Mechanical	Withstand vibration and shock loads during all mission phases
Thermal	Withstand temperatures from -125°C to 125°C

extracting samples from the Martian underground down to a depth of 2 m (Vago et al., 2018), far deeper than Curiosity’s drill (Okon, 2010; Vaniman et al., 2014).

The here proposed antenna system is arranged so that two orthogonal linear polarized waves can be transmitted *and* received separately, yielding a set of four different measurements, which carry additional information on the polarization changes the wave experiences while travelling through the subsurface. These capabilities allow greatly improved analysis of underground structures and target classification (Lu et al., 2017).

2. Requirements and design

The antenna design is driven by requirements that are derived from the WISDOM instrument itself. This includes the electrical parameters of the antenna, as well as the specification due to the mission environment, such as the mechanical framework and the temperature variations. Table 1 gives an overview about the specifications considered for the antenna design. Compared to the initial requirements given in Ciarletti et al. (2011) there are only changes in structural requirements due to change of launcher. The scientific goals were not altered.

2.1. Electrical parameters

The bandwidth of 2.5 GHz allows a depth resolution of around 6 cm in free space. Assuming a relative permittivity ϵ_r of 4, the resolution is enhanced to 3 cm. For the absolute frequency limits, a trade-off between the antenna size and the penetration depth has to be performed. Setting the lower limit to 500 MHz gives a size of antenna’s aperture of around 30 cm if one takes a half wavelength as a basis for the design. The frequency range is chosen so, that the penetration depth is at least three meters under expected nominal conditions, i. e., in dry soil, defined as containing less than 5 wt% of water (Leshin et al., 2013).

All electrical parameters need to be fulfilled over the whole frequency band.

Considering the input RF power, the WAA has to support an amount of 100 mW RF power. For other environments (e. g. on moon) and a higher RF power, an assessment on multipaction and/or corona discharge effects might be necessary. As the WAA does not contain any active components, no additional (DC) power has to be supplied.

Another important set of specifications are given by the so called S-parameters, where the “S” means “scattering”. In general terms, these

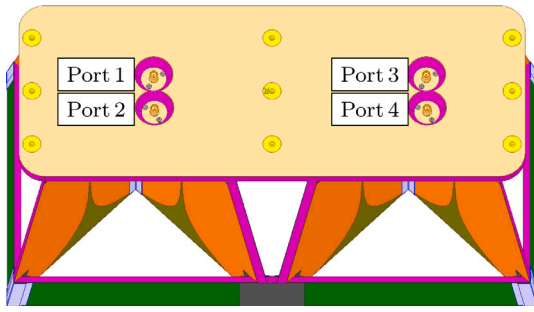


Fig. 2. Top view of the antenna with the numbering of ports: Port 1 and Port 2 are for the transmitting antenna elements, Port 3 and Port 4 are for the receiving elements.

parameters are used to describe the electrical behaviour of linear networks, especially for high-frequency applications. The here presented antenna is such a network with four connectors (from now on called ports) as is shown in Fig. 2. The S-parameter have the form $S_{i,j}$, which simply means: What comes out at port i (amplitude and phase of e. g. a voltage wave) compared to what is put in at port j , when there is no input at all other ports $k \neq j$. Formally, this is written as (Pozar, 2011):

$$S_{ij} = \left. \frac{V_i^-}{V_j^+} \right|_{V_k^+ = 0 \text{ for } k \neq j} \quad (1)$$

For instance, if we send a voltage wave V_1^+ to port 1 and look at the reflected wave V_1^- at this port, then we can calculate S_{11} , which is called the reflection coefficient. If the S-parameter describes a reflection coefficient (S_{nn}), the lower the value the more energy is accepted at that port, which is the preferred behaviour, since this is a prerequisite to radiate most of the available power. Also, if the S-parameter describes a direct coupling from transmitting to receiving antenna, a low value is of high interest.

For the proposed antenna, a reference value S_{nn} of -10 dB is used at all ports, which means that 10% of the RF power can be reflected at the antenna port. In the following, this reflection coefficient is always considered with respect to a 50Ω system.

In order to characterize the subsurface in terms of polarization effects, two separate and orthogonal, linear polarizations need to be transmitted and received by the antenna system. Hence, separate antennas for transmission and reception are necessary. Since transmitter and receiver operate simultaneously, a part of the radiated power is directly transmitted to the receiver. This unwanted direct coupling reduces the dynamic range available for the useful signal coming from the (sub-) surface. Hence, this part should be minimized.

Considering the antenna pattern, the following requirements drive the antenna's design:

- **Gain in main beam direction** (referred to as gain hereafter if not stated otherwise). Gain should increase with frequency, as loss due to the properties of the sounded materials (per unit of distance) and spreading loss increase with frequency. A gain of > 0 dBi partly compensates for the spreading loss (Friis, 1946).
- **General shape:** For the WISDOM instrument, it is advantageous to have a wide beam in the H-plane and a narrow one in the E-plane over the whole frequency range, as this allows a sampling as shown in Fig. 3.
- **Half-Power Beam Width (HPBW):** This is the angle of the direction relative to the main lobe direction, where the radiated power is halved. If the height over ground is 38 cm (which is the case with the ExoMars-Rover) the minimum HPBW of 20° yields a sufficient overlapping of an ideal footprint ellipse as indicated in Fig. 3.

Where applicable, the antenna parameters are given with respect to the far field of the antenna. This is a region, where the shape of the radiation pattern is independent of the distance to the antenna and

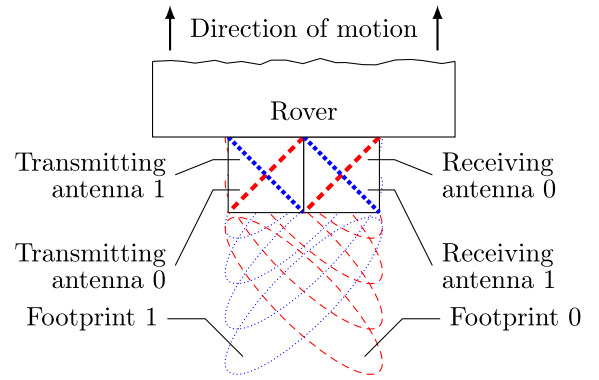


Fig. 3. Scanning scheme that can be achieved with the WAA design; view from above, not to scale.

the electromagnetic wave is a plane wave (Balanis, 2005). Conversely, the near field surrounds the antenna immediately but here the pattern depends on the distance, where it is recorded. Therefore, the pattern in far field is primarily used for comparing antennas. In theory, the far field is given at infinite distance. Consequently, an error must be accepted for practical measurements. In this paper, the pattern is measured in near field and the data is transformed to far field (Johnson et al., 1973). The gain measurement is based on a minimum distance as defined in Bansal (1999).

2.2. Environmental parameters

The environmental requirements are defined by mission and operational constraints. They ensure feasibility of the cruise to and landing on Mars and safe rover operations. They define the general framework within which the electrical antenna design must be realized. Some of the electrical requirements had to be relaxed to fulfil the mechanical parameters. This is discussed below.

The temperature range that the antenna has to withstand is bounded by the following two requirements: Since the antenna is mounted on the outside of the Rover, it is exposed to the Martian atmosphere. No thermal control unit was planned for the WAA, therefore, a minimum temperature of -120°C must be tolerated (Tillman, 2001; Tillman et al., 1994; Kieffer, 1976). In contrast, the maximum temperature of 125°C is defined by the Dry-Heat Microbial Reduction (DHMR) procedure. Here, the antenna is treated with dry hot air (maximum water content 1.2 g/kg) for a duration of three hours on that temperature. This procedure is required for the purpose of planetary protection and inactivates a population of microorganisms by three magnitudes, i. e., 99.9%.

With the requirements outlined above, the Vivaldi antenna design (Gibson, 1979) was chosen as the foundation for the WAA (Plettemeier et al., 2009a,b): A Printed Circuit Board (PCB) based design made of a single copper layer laminated onto a Glass-fiber Reinforced Plastic (GFRP) substrate is used, and the reverse side hosts the feeding structure. The copper is coated with gold to prevent it from oxidizing.

To circumvent the challenges of crossing a single Vivaldi slot antenna, which are

- placing the feedings points of both antenna blades at the same place and
- aligning the small slots properly,

an array of two Vivaldi structures on a single PCB, as shown in Fig. 4, was created.

A useful side effect of this approach is a reduced height compared to a single slot variant. This design again needs less stiffening structures, since the first mechanical self-resonance is shifted towards a higher frequency.

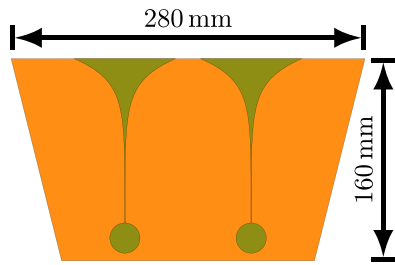


Fig. 4. Design of the basic element for the WISDOM antenna, consisting of two Vivaldi tapered slot antennas. The PCB is made of a substrate (olive-green) that carries the metal layer (orange). The feeding structure on the backside is shown in the following Fig. 5.

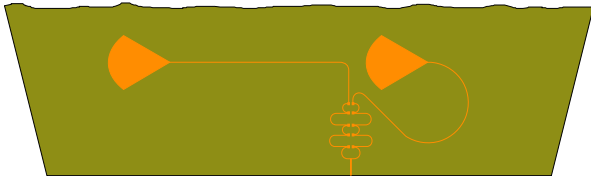


Fig. 5. Two-element array reverse side (detailed view) with the principal divider and feeding structure.

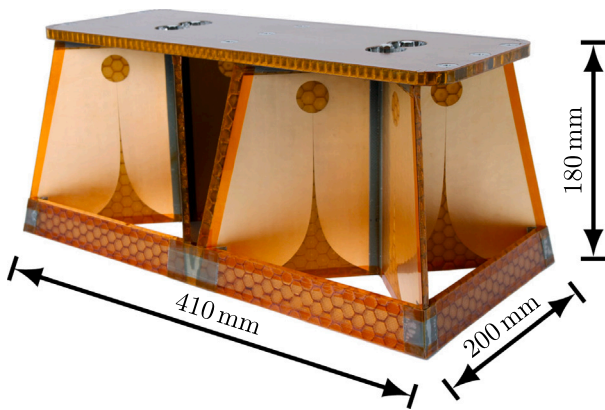
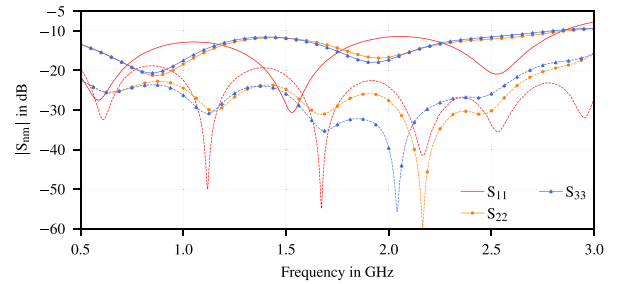


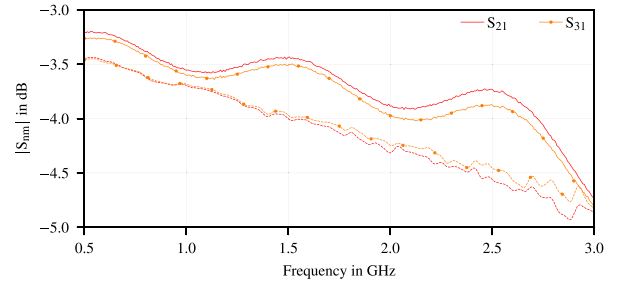
Fig. 6. Final model of the WISDOM Antennas Assembly.

The two-element array design, of course, has two feeding points, and therefore needs an additional power divider/combiner. Initially, a classic five-stage Wilkinson divider (Wilkinson, 1960) was implemented (Benedix et al., 2013). It was etched onto the same substrate as the antenna structure itself, then bent by 90°, and glued onto the baseplate, in order to comply to the spatial dimension requirements for the WAA. However, the microstrip lines connecting the divider with the feed points were very sensitive to the manufacturing process and broke easily, causing disconnect, and thereby complete loss of functionality. After a trade-off analysis between reliability, size and electrical parameters, a final version, shown in Fig. 5, is used. It is much smaller and fits on the antenna blade without bending. Due to the shorter microstrip lines, the losses are lower (i. e., higher transmission) for the small divider, as can be seen in Fig. 7(b). Reflection coefficients for any port n (S_{nn}) as shown in Fig. 7(a) are acceptable but higher than for the first design.

The overall mechanical design presented in Fig. 6 consists of lightweight-construction plates with a honeycomb support shape used to strengthen the antenna elements as well as the baseplate. All reinforcement is made of GFRP, except for the baseplate, where aluminium honeycomb with 6 mm spacing was used. An additional frame around the lower end of the antenna further stiffens the structure and enhances



(a) Reflection coefficient and crosstalk of the old (dashed lines) and new (solid lines) divider.



(b) Transmission of the old (dashed lines) and new (solid lines) divider.

Fig. 7. Measured scattering parameters of the used power divider/combiner compared to a former, larger design.

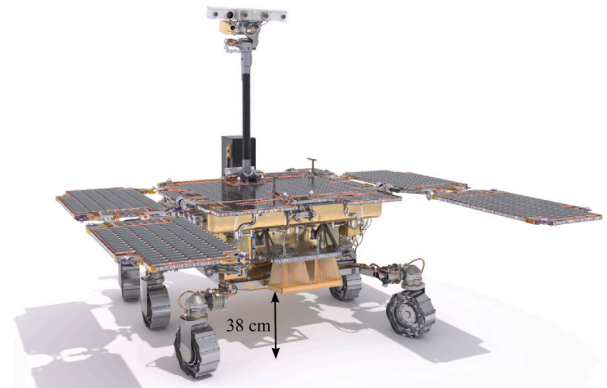


Fig. 8. The WISDOM antenna is placed at the rear of the Rosalind Franklin Rover. In nominal condition, the antenna aperture is located 38 cm above ground. Modified capture from ExoMars Rosalind Franklin (2020).

stability. The antenna is mounted by nine screws (M5) from the top side. For this, nine steel inserts are bonded into the baseplate. This stiff and reliable construction (as the results of the environmental tests show in Section 4) sums up to a total weight of 535 g. The antenna placement at the rear of the rover is shown in Fig. 8.

For the sake of simplicity and to save mass, we decided to go without a cover, initially designed to protect the WAA from the Martian dust. This decision is supported by an experiment, where the influence of dust on the antenna performance was investigated. The basic idea of this experiment is to set up two single antenna blades facing to each other, polarization matched in far-field. Fig. 9(a) shows one of the two blades in the original state. After an accurate initial characterization of the transfer function of the clean blade, a series of measurements have been performed with the blade covered with dust. The Mars-like regolith MRS (Mars Regolith Simulant Allen et al., 1997) is used for two different configurations: a thick layer where the blade is totally covered with dust as shown in Fig. 9(b) and a thinner one where the

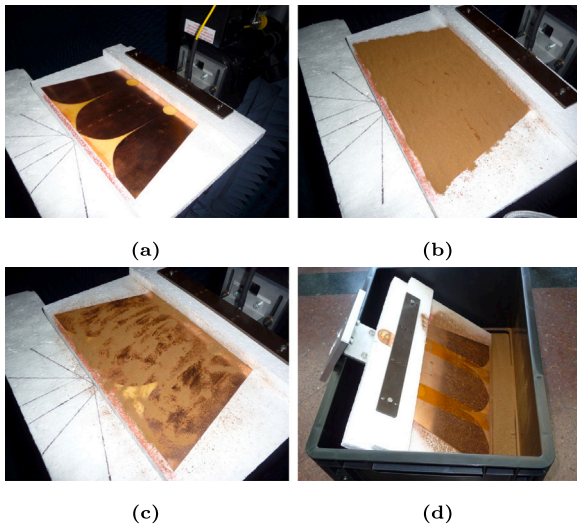


Fig. 9. Experimental investigation of the influence of Mars dust on the antenna performance: (a) Original state of an antenna blade; (b) thick layer and (c) thin layer of MRS on the antenna blade; (d) Test of the accumulation of dust on a slanted antenna blade.

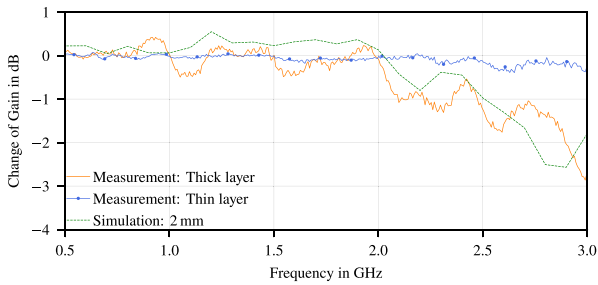


Fig. 10. Influence of different MRS-layers on the antenna gain.

blade is only partially covered (see Fig. 9(c)). The change in the transfer function is recorded in each case. This change represents the difference of gain in the main direction normalized by the value measured on a clean blade and is presented in Fig. 10. We see that the effect of the dust is very limited (less than 0.3 dB) for the thin layer and that, for a thicker layer, the effect is more important (up to almost 3 dB) especially at frequencies higher than 2 GHz. Here, a thick layer of MRS reduces the gain by almost 3 dB at 3 GHz. This frequency dependent behaviour (decrease of gain with increasing frequency) can be simulated by modelling a 2 mm thick layer of material with a permittivity ϵ_r of 4 and dielectric losses $\tan \delta$ of 10^{-2} , which gives the best match to the measured values. However, a thin layer as in Fig. 9(c) reduces the gain less than 0.5 dB. To test how thick a layer of dust on the antenna might grow, the blade was placed at an angle in a container and sprinkled with MRS, as in Fig. 9(d). Even under this oblique arrangement, only a little MRS remains. In conclusion, we are confident dust will not have any significant effect on the antennas performances.

3. Electrical characteristics – Simulation and test

The knowledge of the antenna parameters like gain, pattern and direct coupling is mandatory for modelling the behaviour of the GPR and hence, for interpreting the data gathered during surveys (Hervé et al., 2020).

This section covers the electromagnetic (EM) behaviour of the WAA, from simulations as well as from measurements. ANSYS HFSS was used for the EM simulations, a software tool based on the Finite Elements Method (FEM) (Van Rienen, 2001).

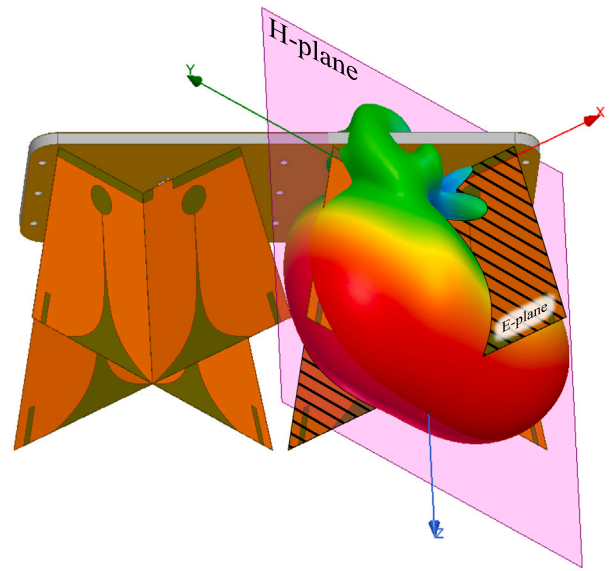


Fig. 11. WAA simplified EM simulation model with a 3D-pattern at 2 GHz that is produced by the hatched antenna blade. For the later shown pattern, the cut of this pattern by the pink plane is the H-plane, while the E-plane coincides with the hatched blade.

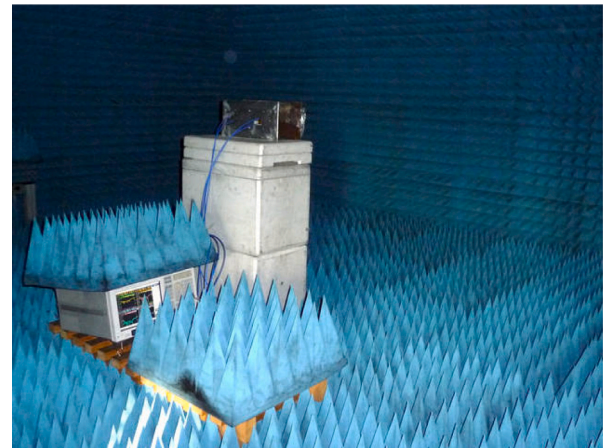


Fig. 12. WAA measurement setup for reflection coefficient. The antenna is placed on top of a polystyrene tower facing to the absorber wall in a distance of 2.4 m.

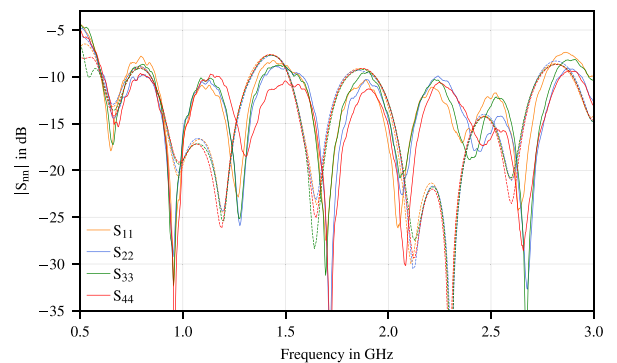


Fig. 13. Reflection coefficient of all four ports, simulated (dashed lines) and measured (solid lines).

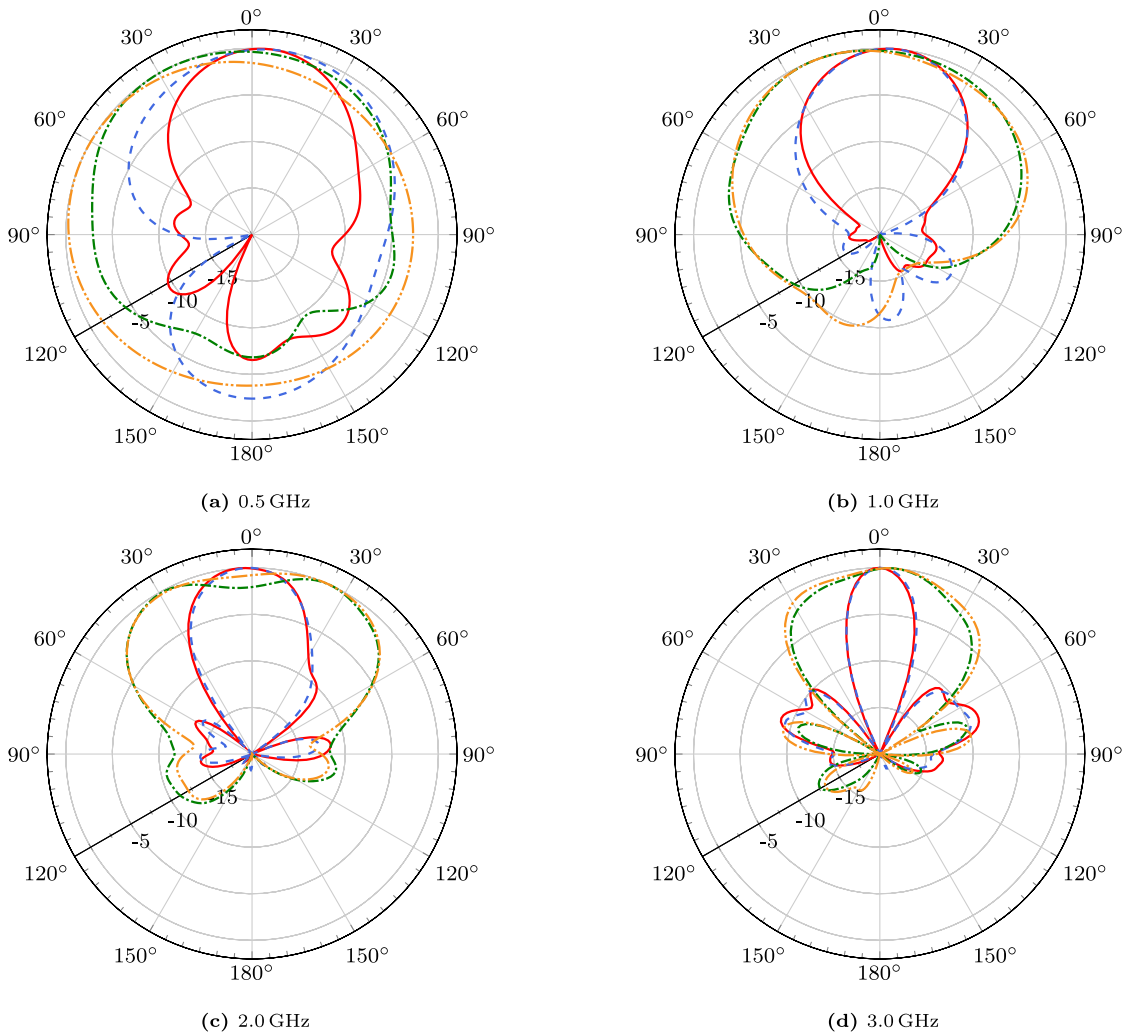


Fig. 14. Normalized antenna pattern (in dB) of Port1 in both principal planes: — measured E-plane, - - simulated E-plane, - - measured H-plane and - - simulated H-plane.

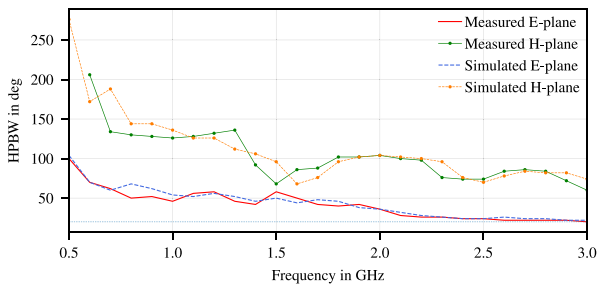


Fig. 15. Measured and simulated HPBW of Port1 of the WAA. The horizontal line at 20° is the requested minimum.

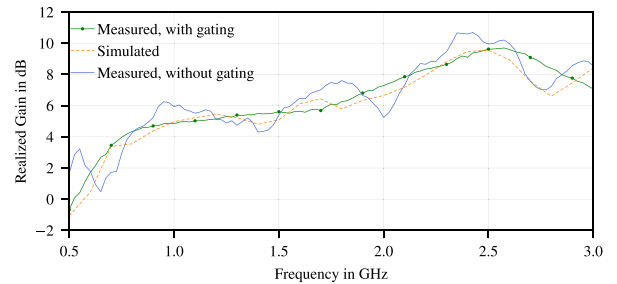


Fig. 16. Measured and simulated realized gain of the antenna blade fed from Port1 of the WAA.

Simulations were run with a simplified model as shown in Fig. 11. In order to reduce computational resources, the following simplifications are applied:

- The GFRP honeycomb support frame was omitted. Due to the low volume fraction and low relative permittivity of GFRP (Mumby et al., 1989), the influence of this frame on the general result is expected to be low to negligible.
- The 3D copper layers were replaced by sheet elements of finite conductivity. It is common practice to approximate very thin metallic structures by sheets, i.e., elements with zero thickness, in simulation setups.

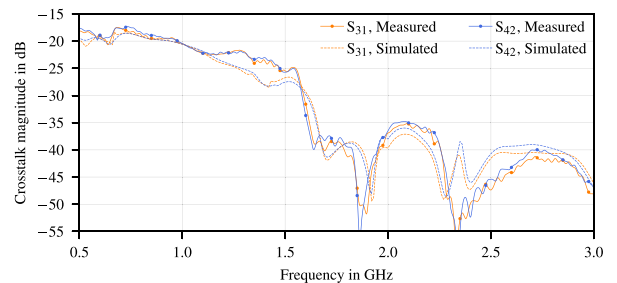


Fig. 17. Measured and simulated coupling of the WAA.

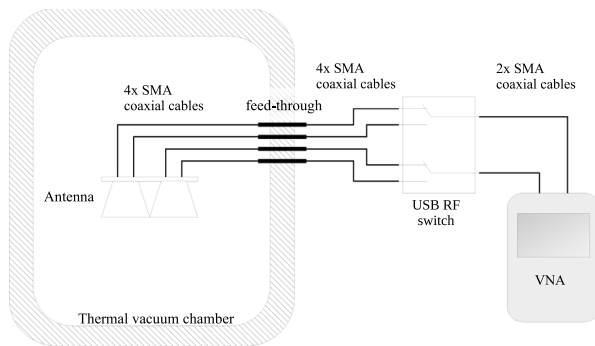


Fig. 18. Setup to measure the reflection coefficient during thermal cycling.

- The baseplate aluminium honeycomb was replaced by solid aluminium. The honeycomb spacing of 6 mm does not influence the EM properties in the considered frequency range, it effectively functions as a reflective wire screen (White, 1980).
- The coaxial feed connector was replaced by a simple microstrip feeding, as both can be assumed to be reasonably well-matched.

For the measurement of the antenna parameters, the so called Flight Model (FM) was used, which is the model that has been integrated to the Rosalind Franklin Rover. This model is identical in construction with the EQM, that has been used for environmental testing in Section 4.

3.1. Scattering parameters

Measurements for reflections and coupling were carried out in the anechoic chamber of the RF Chair at TU Dresden. As shown in Fig. 12, the WAA was placed onto a tower of polystyrene boxes as mechanical support. The boxes' influence on the electromagnetic behaviour of the antenna can be neglected in the investigated frequency range. The main beam is directed to the absorber wall at a distance of 2.4 m, which is beyond the calculated minimum far-field distance of 1.57 m at 3 GHz according to Bansal (1999). With a 4-port Agilent E8364B Vector Network Analyzer (VNA), the S-parameters were recorded after all environmental tests including Long Term Thermal Vacuum (LTTV) were executed.

The measured values are presented in Fig. 13 and are compared to simulated values (dashed lines). The reflection coefficient reaches -5 dB in the range from 0.5 GHz to 0.6 GHz, which is caused by the power divider. In the remaining frequency range up to 3 GHz, the reflection coefficient on Port 1 is -7 dB at worst. The reflection coefficient on the other ports is better than -8 dB. The frequency shift can be explained by the differences between the simulation model and the real model, as described above.

3.2. Antenna pattern

The patterns were measured with a spherical near-field scanner NSI 700-30 in combination with an Agilent E8361A VNA in the same anechoic chamber. For the probe antenna, an RFspin DRH 400 was employed. The results are shown in Fig. 14. Here, simulated and measured antenna pattern at several frequency points in both E- and H-plane are presented.

These pattern show a wide H-plane and narrow E-plane as required in Section 2. Around the centre frequency (see pattern for 1 GHz and 2 GHz) the deviation between measurement and simulation is negligible, especially towards the main beam direction. Although a simple Vivaldi antenna would exhibit a symmetrical pattern, here the proximity of the transmitting and receiving antennas distorts the pattern. Compared to the higher frequencies, the radiation characteristics at 0.5 GHz indicates a larger deviation between simulation and

Table 2

Achieved values of the WISDOM antenna.

Electrical parameters achieved	
Frequency range	0.5 GHz to 3.0 GHz, all following parameters are considered over that frequency range.
Input RF power	20 dBm $\hat{=}$ 100 mW, achieved by design. The used resistors can be loaded up to 100 mW.
Reflection on a 50 Ω line ($ S_{11} $)	< -4.4 dB at 0.5 GHz at Port 1, all other ports are below over the frequency range, see Fig. 13
Direct coupling	< -17.3 dB, see Fig. 17
Polarization	Two linear, perpendicular polarizations are achieved by design.
Antenna pattern	Above 1 GHz there is a clear directional, homogeneous main lobe, see Fig. 14.
HPBW	$\theta \geq 20^\circ$, $\theta_{H\text{-plane}} > \theta_{E\text{-plane}}$, see Fig. 15
Gain in main beam direction	> -0.7 dBi at 0.5 GHz at Port 3, increasing with frequency up to 2.6 GHz, see Fig. 16
Structural & environmental parameters achieved	
Mass	535 g
Envelope	410 \times 199 \times 178 mm
First mechanical eigenfrequency	347 Hz, see Fig. 23
Mechanical	Passed all vibration and shock tests
Thermal	Passed all thermal vacuum tests, see Fig. 21(b) and Fig. 25

measurement, especially in the E-plane. This is most probably caused by coupling with the spherical scanning system and performance degradation of the anechoic chamber below 1 GHz. At around 2 GHz, side lobes begin to arise and become a comparatively large portion of the pattern at 3 GHz. That in turn decreases the power to the main beam direction. In Fig. 15, the measured HPBW of Port 1 is plotted versus frequency for both E- and H-plane and is compared to the simulation results. The plots of simulated and measured data show a similar shape with an acceptable deviation.

3.3. Realized gain

Measurements were performed in the anechoic chamber with an Agilent FieldFox N9918A VNA, employing the well-known three-antenna method (Balanis, 2005). The results of these measurements are shown in Fig. 16, together with simulation results. Again, due to the imperfections of the anechoic chamber the probe antenna receives the signal via multiple transmission paths, causing clearly visible interference. This leads to strong deviations compared to the simulation results. By applying a time gating algorithm (in the VNA), the indirect paths are suppressed, and the graph is much smoother, and also in much better agreement with the simulation results. Realized gain is increasing with frequency up to 2.6 GHz, which is wanted to reduce spreading (i. e., free space loss) and material losses. Above this frequency, the side lobe power becomes so high that the power in main beam direction decreases.

3.4. Direct coupling

Direct coupling between transmitting and receiving antenna should be as low as possible to improve the dynamic range of the system on one hand. On the other hand, direct coupling is the earliest signal that is received through the antennas and most of the time the strongest one, which gives a reliable signal for long term reference being on Mars.

Simulation and measurement results are shown in Fig. 17. As can be seen, in the lower band from 0.5 GHz to 1.6 GHz the coupling is within the range from around -20 dB to -25 dB, with a maximum of approx. -17.3 dB at 0.7 GHz. At about 1.6 GHz, there is a sharp decline. Until up to the nominal maximum frequency of 3 GHz the coupling is -34 dB at worst.

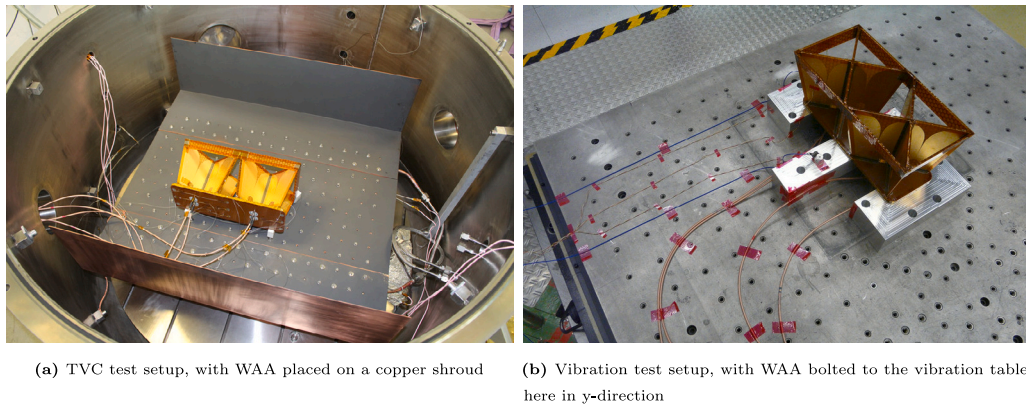


Fig. 19. Environmental test setups.

4. Qualification

The qualification process encompasses assessments of the materials and manufacturing processes, as well as environmental tests. The antenna has to withstand several stress tests, such as thermal cycling and mechanical loads. For this purpose the EQM was used. For the sake of clarity, the following diagrams only show a representative section of the measurements.

4.1. Thermal cycling

For the thermal environment qualification, the EQM shall withstand 130°C and -130°C , which is the requested temperature range with an extra qualification margin of $\pm 10\text{K}$. In total, eight cycles have to be passed.

While the first cycle spans the full temperature range at below 1mPa , the subsequent cycles simulate a Mars analogue atmosphere at 700Pa of Nitrogen with a reduced maximum temperature of 80°C . The duration at the hottest/coldest points is composed by three states, which are: (1) initial stabilization, where the target temperature is reached within $\pm 0.5^{\circ}\text{C}$, followed by (2) a stabilization phase of four hours, where the temperature shall stay within $\pm 0.25^{\circ}\text{C}$ and (3) an additional dwell time of 2 h. The test was done in a Thermal Vacuum Chamber (TVC) as shown in Figs. 20 and 19(a) shows the plots of temperature and pressure during that qualification test.

Before and after the full test, as well as after each dwell time, the reflection coefficient was measured with a setup illustrated in Fig. 18. Via a feed-through, the ports of the antenna inside the thermal vacuum chamber are connected to an Agilent N9918 VNA outside. An RF switch enables the sequential measurement of all four antenna ports with the two ports of the VNA.

Fig. 21(a) shows the measured values of the reflection coefficient on Port 1 during the first cycle. Compared to the measurement of reflection coefficient within the anechoic chamber, this time the antenna is surrounded by the metallic vessel of the TVC within the near-field of the antenna. Hence, due to reflections at these metallic walls, the values differ significantly from those taken in the anechoic chamber (compare with Fig. 13). Therefore, these values can only be considered as a health status rather than a reference for GPR post-processing.

The reflection coefficient on Port 1 at ambient temperature together with the maximum values of all hot and cold measurements is shown in Fig. 21(b), giving an estimate of the expected worst case behaviour. Although the difference is as much as 3dB at 0.8GHz , the total magnitude is always lower than -3dB , which is considered acceptable.

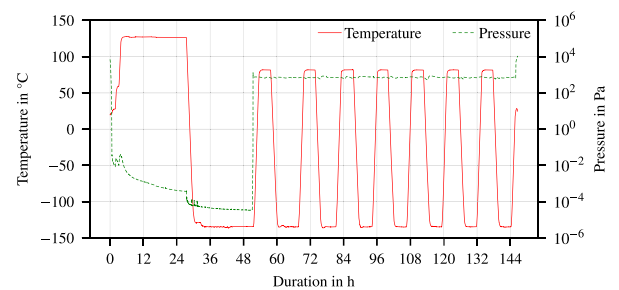


Fig. 20. Temperature and pressure during the thermal qualification test of the EQM.

4.2. Vibration

Fig. 19(b) shows one of the arrangements for the mechanical vibration tests that consist of sinusoidal and random excitations along all three axes. From simulations results of the mechanical behaviour, three spots (stiffest/most fragile) on the structure were chosen to be monitored with accelerometers, as can be seen in Fig. 22.

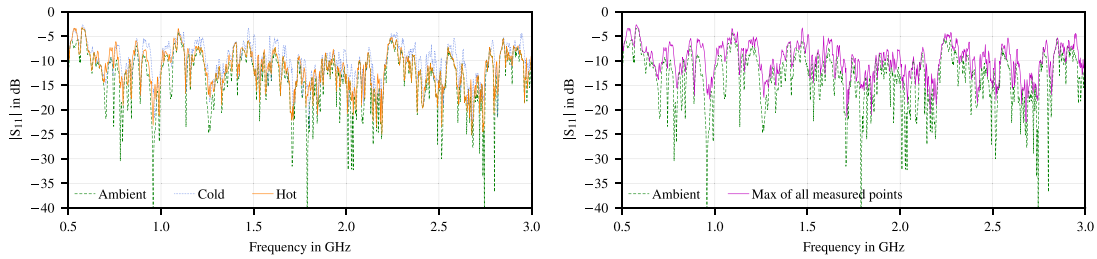
Between each single load test a resonance search was performed, the antenna structure was checked visually, and the functionality was again checked by measuring the reflection coefficient. In this case, the resonance search was a sinusoidal sweep from 5Hz to 2000Hz . This allows the natural frequencies to be recognized. In addition, one can detect changes in the structure, which may be caused by any of the load tests. As shown in Fig. 23, the difference between initial and final resonance search is negligible, which means that the antenna structure has got no damages due to those load tests.

Another test was the shock test, which will not be outlined in this article, since the procedure is similar to that of the vibration test. Here, the antenna is exposed to a short impact, that has to fulfil a given acceleration spectrum.

4.3. Long term thermal test

Furthermore, a long term cycling test was performed. The aim of this test was to verify that the WISDOM antenna survives the planned life span. To achieve this, the antenna was exposed to 327 cycles (218 sols extended mission time multiplied by a safety factor of 1.5) under a Mars analogue atmosphere with 700Pa of Nitrogen atmosphere. This test was carried out in a smaller TVC than for the qualification test, see Fig. 24.

The temperature range was set between 75°C (hot point) and -125°C (cold point). The dwell time was reduced to 15 min only, since in this test the transitions between hot and cold points was the main focus. During the test, the transition rate was set to 6Kmin^{-1} . With all these settings, the test ran for almost 75 days.



(a) Magnitude of reflection coefficient on Port 1 of ambient, hot and cold temperature measurement (first cycle), TVC closed (b) Magnitude of reflection coefficient on Port 1 of ambient temperature and the maximum values of all cycles

Fig. 21. Results of reflection coefficient measurement during thermal cycling.

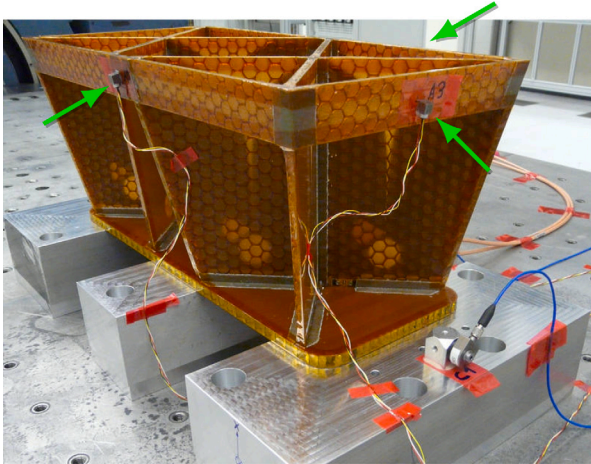


Fig. 22. Vibration test of the WAA; arrows point at accelerometers. The third accelerometer is on the far side, in the middle of the strut.

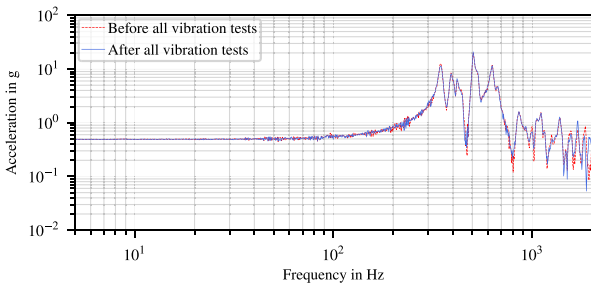


Fig. 23. Resonance search of the antenna structure before and after all vibration tests. The plot shows the acceleration at sensor A3 (see Fig. 22) in y direction. The first resonance frequency appears at around 347Hz, which is far beyond the critical point of 140 Hz.

Throughout the entire time, a measurement of all four ports was carried out every 5 min to check the antenna’s operational state. In Fig. 25, the reflection coefficient on Port 1 of the first measurement (ambient) is plotted. A second graph shows the maximum magnitude that occurred during the whole test for each single frequency, in order to check for failures. If a failure (e. g. interrupted or short-circuited line) had occurred, this would have resulted in a maximum value of 0 dB, which is not the case. The reflection coefficient behaves differently compared to that recorded during the qualification, since this chamber is much smaller.

After all environmental tests, a measurement of the scattering parameters was done in the anechoic chamber and compared to the state before all tests. Fig. 26 shows the reflection coefficient at Port 1 before and after testing. As can be seen, the impact of all tests on the reflection

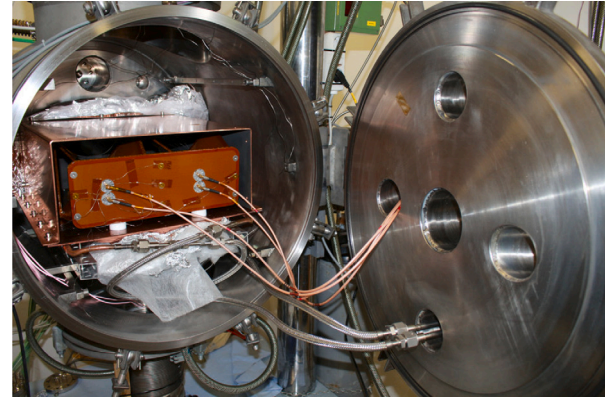


Fig. 24. The EQM installed in the smaller TVC for the Long Term Thermal Cycling.

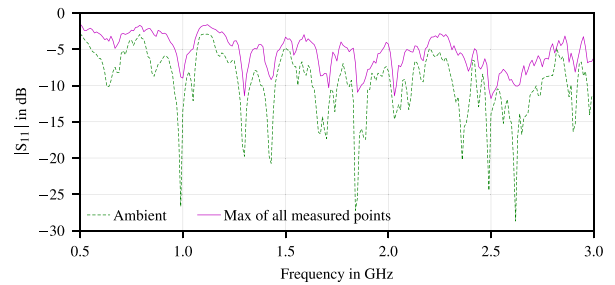


Fig. 25. Magnitude of reflection coefficient on Port 1 both for ambient temperature and for the maximum value (of each frequency point) that occurred during the whole long term thermal cycling.

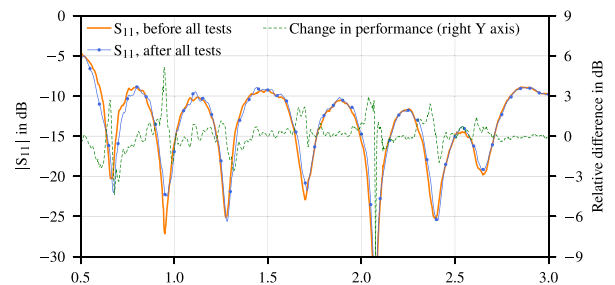


Fig. 26. Measurement of the reflection coefficient on Port 1 in anechoic chamber before and after all environmental tests: thermal-vacuum, vibration, shock and long-term thermal cycling.

coefficient is low enough to be accepted: in regions where $S_{11} > -10$ dB the performance degradation is below 1 dB at worst.

The EQM passed all environmental tests without any issues.

5. Conclusion

Besides the ordinary design goals for GPR-antennas, the construction of a rover based space antenna has to deal with a number of further challenges, such as the electrical large gap between antenna and ground, mechanically stable construction, and usage of space qualified materials.

The achieved values for the given requirements from Table 1 are summarized in Table 2. The matching is not fully compliant to the requirement of < -10 dB. The impact will be that at some frequencies the returned signal power is higher than required. Therefore, the realized gain is lower at these ranges. For the RF components of the WISDOM electronic unit, this higher returned power is not an issue, however.

The lowest realized gain is around 0.7 dB below the requested value of 0 dBi at the lower frequency limit. Further, it was required that the gain in main beam direction shall increase with frequency to compensate for the increasing loss. Up to 2.6 GHz this is achieved. Because of increasing side lobes above that frequency, the gain decreases. This behaviour will be compensated by calibrating the whole system with the cost of some dynamic loss.

In this paper we presented the basic design and the antenna parameters – both of simulation and measurement – such as reflection coefficient, pattern, gain, and coupling of the WISDOM GPR antenna for the ExoMars Rover. As outlined in detail, the antenna passed all required tests for space environment.

CRediT authorship contribution statement

Wolf-Stefan Benedix: Writing – original draft, Investigation, Funding acquisition, Data curation. **Sebastian Hegler:** Writing – review & editing, Visualization, Software, Data curation. **Christoph Statz:** Writing – review & editing, Data curation. **Ronny Hahnel:** Writing – review & editing, Investigation. **Dirk Plettemeier:** Supervision, Project administration, Funding acquisition, Writing – review & editing, Conceptualization. **Valérie Ciarletti:** Writing – review & editing, Supervision, Conceptualization.

Funding

The research on the WISDOM experiment is supported by funding from Bundesministerium für Wirtschaft und Klimaschutz under contract 50QX2301. The work is supported by the German Aerospace Center (Deutsches Zentrum für Luft- und Raumfahrt e. V., DLR) and the National Center for Space Studies (Centre national d'études spatiales, CNES).

Declaration of competing interest

The authors declare that they have no known competing financial interests or personal relationships that could have appeared to influence the work reported in this paper.

Acknowledgements

This antenna assembly would not be reality without the constructive collaboration with Invent GmbH, Braunschweig and Contag AG, Berlin. We would like to thank all members of the WISDOM team who have supported the development, measurement, and test of the antenna.

Data availability

Data will be made available on request.

References

- Allen, C.C., Morris, R.V., Lindstrom, D.J., Lindstrom, M.M., Lockwood, J.P., 1997. JSC mars-1 - martian regolith simulant. In: Lunar and Planetary Science Conference. In: Lunar and Planetary Inst. Technical Report, vol. 28, p. 27.
- Balanis, C.A., 2005. Antenna Theory. Analysis and Design, third ed. Wiley & Sons, ISBN: 0-471-66782-X.
- Bansal, R., 1999. The far-field: how far is far enough? Appl. Microw. Wirel. 11 (11), 59–60.
- Benedix, W.S., Plettemeier, D., Zaroni, A., Preller, F., Ciarletti, V., 2013. Advance of WISDOM GPR antenna for ExoMars 2018 mission. In: Wireless for Space and Extreme Environments (WiSEE), 2013 IEEE International Conference on. pp. 1–3, doi: 10/gfzj54.
- Ciarletti, V., 2016. A variety of radars designed to explore the hidden structures and properties of the solar system's planets and bodies. Probing Matter with Electromagnetic Waves/Sonder La Matière Par Les Ondes Électromagnétiques URSI-France 2015 Scientific Days – Paris, CNAM, 24 & 25 March 2015, Comptes Rendus Phys. (ISSN: 1631-0705) Probing Matter with Electromagnetic Waves/Sonder La Matière Par Les Ondes Électromagnétiques URSI-France 2015 Scientific Days – Paris, CNAM, 24 & 25 March 2015, 17 (9), 966–975. doi: 10/f86h7m.
- Ciarletti, V., Clifford, S., Plettemeier, D., Le Gall, A., Hervé, Y., Dorizon, S., Quantin-Nataf, C., Benedix, W.-S., Schwenzer, S., Pettinelli, E., Heggy, E., Herique, A., Berthelot, J.-J., Kofman, W., Vago, J.L., Hamran, S.-E., the WISDOM Team, 2017. The WISDOM radar: unveiling the subsurface beneath the ExoMars rover and identifying the best locations for drilling. Astrobiol. 17 (6–7), 565–584, doi: 10/gbt8cc.
- Ciarletti, V., Corbel, C., Plettemeier, D., Cais, P., Clifford, S., Hamran, S.-E., 2011. WISDOM GPR designed for shallow and high-resolution sounding of the martian subsurface. Proc. IEEE (ISSN: 0018-9219) 99 (5), 824–836, doi: 10/b5shjw.
- Daniels, D.J. (Ed.), 2004. Ground penetrating radar, second. ed. IEE Radar, Sonar, Navigation and Avionics Series ; 15, Institution of Electrical Engineers, London, ISBN: 0-86341-360-9.
- European Space Agency, 2019a. ESA's mars rover has a name – rosalind franklin. In: ESA's Mars Rover Has a Name – Rosalind Franklin.
- European Space Agency, 2019b. Scientific objectives of the ExoMars rover. In: ESA - Robotic Exploration of Mars - Scientific objectives of the ExoMars rover.
2020. ExoMars rosalind franklin rover 360°. https://www.esa.int/ESA_Multimedia/Videos/2020/03/ExoMars_Rosalind_Franklin_rover_3601/lang.
- Fang, G.-Y., Zhou, B., Ji, Y.-C., Zhang, Q.-Y., Shen, S.-X., Li, Y.-X., Guan, H.-F., Tang, C.-J., Gao, Y.-Z., Lu, W., Ye, S.-B., Han, H.-D., Zheng, J., Wang, S.-Z., 2014. Lunar penetrating radar onboard the chang'e-3 mission. Res. Astron. Astrophys. (ISSN: 1674-4527) 14 (12), 1607–1622, doi: 10/gh2jz9.
- Flamini, E., Fois, F., Calabrese, D., Bombaci, O., Cattoalò, C., Croce, A., Croci, R., Gueffi, M., Zampolini, E., Picardi, G., Seu, R., Mecozzi, R., Biccari, D., Cartacci, M., Cicchetti, A., Masdea, A., Alberti, G., Maffei, S., Papa, C., 2007. Sounding mars with SHARAD & MARSIS. In: 2007 4th International Workshop on, Advanced Ground Penetrating Radar. pp. 246–251, doi: 10/ddn4hg.
- Friis, H., 1946. A note on a simple transmission formula. Proc. IRE 34 (5), 254–256, doi: 10/b5vk3z.
- Gibson, P.J., 1979. The vivaldi aerial. In: 1979 9th European Microwave Conference. pp. 101–105, doi: 10/b7wzch.
- Hamran, S., Berger, T., Brovoll, S., Damsgård, L., Hellenen, Ø., Øyan, M.J., Amundsen, H.E., Carter, L., Ghent, R., Kohler, J., Mellon, M., Paige, D., Plettemeier, D., Eide, J., 2015. RIMFAX: a GPR for the mars 2020 rover mission. In: 2015 8th International Workshop on Advanced Ground Penetrating Radar (IWAGPR). pp. 1–4, doi: 10/ghfm7b.
- Hamran, S.-E., Paige, D.A., Amundsen, H.E.F., Berger, T., Brovoll, S., Carter, L., Damsgård, L., Dypvik, H., Eide, J., Eide, S., Ghent, R., Hellenen, Ø., Kohler, J., Mellon, M., Nunes, D.C., Plettemeier, D., Rowe, K., Russell, P., Øyan, M.J., 2020. Radar imager for mars' subsurface experiment—RIMFAX. Space Sci. Rev. (ISSN: 1572-9672) 216 (8), 128. <http://dx.doi.org/10.1007/s11214-020-00740-4>.
- Hervé, Y., Ciarletti, V., Le Gall, A., Corbel, C., Hassen-Khodja, R., Benedix, W., Plettemeier, D., Humeau, O., Vieau, A., Lustrement, B., Abbaki, S., Bertran, E., Lapauw, L., Tranier, V., Oudart, N., Vivat, F., Statz, C., Lu, Y., Hegler, S., Hérique, A., 2020. The WISDOM radar on board the ExoMars 2022 rover: characterization and calibration of the flight model. Planet. Space Sci. (ISSN: 0032-0633) 189, 104939, doi: 10/ggzg9b.
- Johnson, R.C., Ecker, H.A., Hollis, J.S., 1973. Determination of far-field antenna patterns from near-field measurements. Proc. IEEE (ISSN: 1558-2256) 61 (12), 1668–1694, doi: 10/djg3k7.
- Kieffer, H.H., 1976. Soil and surface temperatures at the viking landing sites. Science 194 (4271), 1344–1346, doi: 10/cm989j.
- Leshin, L.A., Mahaffy, P.R., Webster, C.R., Cabane, M., Coll, P., Conrad, P.G., Archer, P.D., Atreya, S.K., Brunner, A.E., Buch, A., Eigenbrode, J.L., Fleisch, G.J., Franz, H.B., Freissinet, C., Glavin, D.P., McAdam, A.C., Miller, K.E., Ming, D.W., Morris, R.V., Navarro-González, R., Niles, P.B., Owen, T., Pepin, R.O., Squyres, S., Steele, A., Stern, J.C., Summons, R.E., Sumner, D.Y., Sutter, B., Szopa, C., Teinturier, S., Trainer, M.G., Wray, J.J., Grotzinger, J.P., Team, M.S., 2013. Volatile, isotope, and organic analysis of martian fines with the mars curiosity rover. Science 341 (6153), doi: 10/f3sfrz.

- Li, C., Su, Y., Pettinelli, E., Xing, S., Ding, C., Liu, J., Ren, X., Lauro, S.E., Soldovieri, F., Zeng, X., Gao, X., Chen, W., Dai, S., Liu, D., Zhang, G., Zuo, W., Wen, W., Zhang, Z., Zhang, X., Zhang, H., 2020. The moon's farside shallow subsurface structure unveiled by chang'e-4 lunar penetrating radar. *Sci. Adv.* (ISSN: 2375-2548) 6 (9), eaay6898, doi: 10/dnmx.
- Lu, Y., Statz, C., Benedix, W., Drechsel, F., Hegler, S., Plettemeier, D., 2017. Enhanced GPR target classification by compressed sensing and radar polarimetry. In: 2017 18th International Radar Symposium (IRS). pp. 1–8, doi: 10/gfphq4.
- Mumby, S., Johnson, G., Anderson, E., 1989. Dielectric properties of some PTFE-reinforced thermosetting resin composites. In: Proceedings of the 19th Electrical Electronics Insulation Conference. IEEE, pp. 263–267, doi: 10/b6zqd9.
- Okon, A.B., 2010. Mars science laboratory drill. In: Proceedings of the 40th Aerospace Mechanisms Symposium.
- Plettemeier, D., Ciarletti, V., Hamran, S.-E., Corbel, C., Cais, P., Benedix, W.-S., Wolf, K., Linke, S., Roddecke, S., 2009a. Full polarimetric GPR antenna system aboard the ExoMars rover. In: Radar Conference, 2009 IEEE. (ISSN: 1097-5659) pp. 1–6, doi: 10/dg5qfm.
- Plettemeier, D., Corbel, C., Hamran, S.-E., Ciarletti, V., Benedix, W.-S., Balling, S., Linke, S., 2009b. Ultra light-weight antenna system for full polarimetric GPR applications. In: EUROCON 2009, EUROCON '09. IEEE. pp. 1557–1564, doi: 10/cvbj85.
- Pozar, D.M., 2011. Microwave Engineering, fourth ed. Wiley, Hoboken, NJ, ISBN: 978-0-470-63155-3.
- Tillman, J.E., 2001. Mars: temperature overview. https://www-k12.atmos.washington.edu/k12/resources/mars_data-information/temperature_overview.html.
- Tillman, J.E., Landberg, L., Larsen, S.E., 1994. The boundary layer of mars: fluxes, stability, turbulent spectra, and growth of the mixed layer. *J. Atmos. Sci.* (ISSN: 0022-4928) 51 (12), 1709–1727, doi: 10/cnnqx3.
- Vago, J.L., Coates, A.J., Jaumann, R., Korabely, O., Ciarletti, V., Mitrofanov, I., Josset, J.-L., Westall, F., De Sanctis, M.C., Bibring, J.-P., Rull, F., Goesmann, F., Brinckerhoff, W., Raulin, F., Sef-ton-Nash, E., Svedhem, H., Kminek, G., Rodionov, D., Baglioni, P., The ExoMars Team, 2018. Chapter 12 - searching for traces of life with the ExoMars rover. In: Cabrol, N.A., Grin, E.A. (Eds.), *From Habitability To Life on Mars*. Elsevier, ISBN: 978-0-12-809935-3, pp. 309–347. <http://dx.doi.org/10.1016/B978-0-12-809935-3.00011-6>.
- Van Rienen, U., 2001. Numerical methods in computational electrodynamics: linear systems in practical applications. Lecture Notes in Computational Science and Engineering, Springer, Berlin ; New York, ISBN: 978-3-540-67629-4, 12.
- Vaniman, D.T., Bish, D.L., Ming, D.W., Bristow, T.F., Morris, R.V., Blake, D.F., Chipera, S.J., Morrison, S.M., Treiman, A.H., Rampe, E.B., Rice, M., Achilles, C.N., Grotzinger, J.P., McLennan, S.M., Williams, J., Bell, J.F., Newsom, H.E., Downs, R.T., Maurice, S., Sarrazin, P., Yen, A.S., Morookian, J.M., Farmer, J.D., Stack, K., Milliken, R.E., Ehlmann, B.L., Sumner, D.Y., Berger, G., Crisp, J.A., Hurowitz, J.A., Anderson, R., Des Marais, D.J., Stolper, E.M., Edgett, K.S., Gupta, S., Spanovich, N., 2014. Mineralogy of a mudstone at yellowknife bay, gale crater, mars. *Science* 343 (6169), 1243480, doi: 10/f3sdx.
- White, D.R.J., 1980. Electromagnetic Shielding Materials and Performance, second ed. Don White Consultants, Inc., Gainesville, Virginia, ISBN: 978-0-932263-08-7.
- Wilkinson, E., 1960. An n-way hybrid power divider. *IRE Trans. Microw. Theory Tech.* 8 (1), 116–118, doi: 10/bgz4gc.
- Xiao, Y., Su, Y., Dai, S., Feng, J., Xing, S., Ding, C., Li, C., 2019. Ground experiments of chang'e-5 lunar regolith penetrating radar. *Adv. Space Res.* (ISSN: 0273-1177) 63 (10), 3404–3419, doi: 10/gh2j2m.
- Zhou, B., Shen, S., Lu, W., Liu, Q., Tang, C., Li, S., Fang, G., 2020. The mars rover subsurface penetrating radar onboard China's mars 2020 mission. *Earth Plan. Phys.* 4 (4), 345–354, doi: 10/ghfm7p.